International Journal of Mining and Geo-Engineering

IJMGE

IJMGE 52-1 (2018) 75-86

DOI: 10.22059/ijmge.2017.224804.594654

# Uncertainty assessment of coal quality-tonnage curves through minimum spatial cross-correlation simulation

Babak Sohrabian [a, *], Abdullah Erhan Tercan [b], Rohola Hasanpour [c]

[a] *Department of Mining and Metallurgical Engineering, Urmia University of Technology, Urmia, Iran*

[b] *Mining Engineering Department, Hacettepe University, Ankara, Turkey*

[c] *Institute for Tunnelling and Construction Management, Ruhr-University Bochum, Germany*

Article History:

Received: 10 January 2017,

Revised: 12 August 2017,

Accepted: 13 September 2017.

## ABSTRACT

Coal quality-tonnage curves are helpful tools in optimum mine planning and can be estimated using geostatistical simulation methods. In presence of spatially cross-correlated variables, traditional co-simulation methods are impractical and time-consuming. This paper investigates a factor simulation approach based on minimization of spatial cross-correlations with the objective of modeling spatial relations of coal quality data and estimating the quality-tonnage curves in a part of the Ömerler sector of Tunçbilek coalfield (Turkey). Data come from core samples analyzed for lower calorific value, ash content, and moisture content. Prior to simulation, composite data and coal seam are unfolded and the composites are also detrended . The simulations of the original data are obtained by adding the trend values to the simulated residuals and transforming the unfolded coordinates into the original ones. 100 realizations of the coal attributes are jointly generated by Minimum Spatial Cross-correlation (MSC) simulation method. The MSC-simulations are compared to the results of a widely used joint simulation method based on the minimum/maximum autocorrelation factors (MAF) technique. The comparison shows the advantage of the new proposed method over the MAF technique. MSC-simulations properly reproduce the original data based on the correlation coefficient, cumulative histograms, and auto / cross-variograms. This suggests that the MSC-simulation method can be used in simulation of spatially cross-correlated coal data. The quality-tonnage curve for each realization is calculated and uncertainty associated with tonnage is assessed by using a 95% confidence interval. The assessments show that the tonnage uncertainty depends on the cutoff.

**Keywords :** *Coal, Spatial cross-correlation, Multivariate simulation, Quality-tonnage curves, Minimum/maximum autocorrelation factors*

## 1. Introduction

Coal quality–tonnage curves are graphical representations of recoverable coal resources, which plot the tonnage and mean coal quality values versus the cut-off grade. These curves are used in all phases of a mining project, including resource estimation, mine planning, and production scheduling. The quality–tonnage curves should be estimated from the available data at the stage of resource estimation. At this stage, the data are not dense enough to allow reliable predictions. Therefore, it is desirable to assess the uncertainty of the coal quality–tonnage curves. The aim of the present study is assessing the uncertainty associated with the coal quality-tonnage curves.

Geostatistical simulation allows to model the uncertainty by generating equally probable realizations of the coal seam. For spatially cross-correlated variables such as the coal quality data, it is necessary to reproduce the cross dependencies and auto-correlations. Co-simulation, which considers auto and cross-variograms in its algorithm, has been the traditional method in multivariate studies [1-8]. However, co-simulation is impractical due to difficulties in modeling the auto and cross variograms for a large number of variables. Furthermore, to avoid facing with unsolvable equation systems, the auto/cross variograms should be fitted using the Linear Model of Coregionalization (LMC) regarding the Cauchy–Schwarz inequality [9]. It is a necessary but not a sufficient process, which may interfere with the actual spatial structure of the studied attributes.

A practical alternative to the traditional co-simulation method is to use a factor-based approach that is based on transforming the spatially correlated variables into the orthogonal factors and then simulating each factor independently. For generating such factors, a number of methods are suggested in the literature. Some of these methods such as Principal component analysis [10], minimum/maximum autocorrelation factors (MAF) [11-15], stepwise conditional transformation [16-17], simultaneous diagonalization [18-20], independent components analysis [21-23] are able to remove the linear correlation, and some others, for example, non-linear PCA and non-linear MAF have the ability to deal with nonlinear dependencies [24-27].

Another method is the MSC method, which is appealing due to its ability to minimize several variogram matrices [28]. This method deals with removing the linear correlations and lacks the potential to deal with much more complicated nonlinear relationships.

The present study suggests using the MSC method in assessing the uncertainty of the coal quality-tonnage curves. This method converts the multivariate problem into a series of single-variable equations, which can be easily solved applying the gradient descent algorithm. In contrast to the traditional co-simulation methods, the multivariate simulation uses the minimum spatial cross-correlation (MSC) factors that removes the need for cross-variogram modeling and interfering with data's actual spatial structures. Moreover, the MSC simulation is practical and convenient and it provides reliable results [29].

In this paper, the MSC method is applied to the joint simulation of

* Corresponding author Tel: +984431980314, Fax: +984431980313. *E-mail address:* babak_sohrabian@uut.ac.ir (B. Sohrabian).

multivariate coal quality data for a part of the Ömerler lignite seam of the Tunçbilek coal field (Turkey) for generating the coal quality-tonnage curves. The data comes from core samples of 115 boreholes that are analyzed for Lower Calorific Value (LCV), Ash Content (AC), and Moisture Content (MC). In the area of interest, the coal seam is separated into 7 zones due to faulting. The coal seam is folded and all attributes show significant trends in the vertical direction so that before the application of the MSC approach, the space is unwrinkled and the data is detrended. Then, the MSC is applied to transform the intercorrelated variables into the spatially uncorrelated factors. The factors are simulated independently through the Direct Sequential Simulation (DSS) method. In order to compare the MSC-simulation method with a more widely used multivariate technique, the same process is implemented using the MAF approach. The MSC-simulation shows a better performance than the MAF-simulations in reproducing the statistical properties of data. After adding the trends to the back-transformed simulations, the MSC-simulation results are used to estimate the quality-tonnage curves and to assess the associated uncertainty. The case study shows that the MSC method can be used in constructing the coal quality-tonnage curves. On the other hand, the uncertainty of simulated tonnage curves depends on the cutoff.

The outline of the paper is as follows: the second section gives a brief summary of the joint simulation based on the MSC factors including the concepts and the notations. In the third section, a case study including field and geological setting descriptions, properties of coal variables, data detrending, seam unfolding, joint simulation using the MSC factors, and a comparison to the MAF-simulations are presented. The final section provides the conclusions.

## 2. Methodology

This section provides a brief theory of the MSC-simulation. More details are presented in [29].

### 2.1. Multivariate Simulation using Factors

Suppose Let $\boldsymbol{Z}(\boldsymbol{x}) = [Z_1(\boldsymbol{x}), Z_2(\boldsymbol{x}), \dots, Z_p(\boldsymbol{x})]$ is a $P$ dimensional secondorder stationary random function where $x$ represents the location within a region $D$. Under the second-order stationary assumption, $\boldsymbol{Z}(\boldsymbol{x})$ has a constant mean $\boldsymbol{\mu} = E[\boldsymbol{Z}(\boldsymbol{x})]$ and a variogram matrix

$$2\boldsymbol{\Gamma}_{\boldsymbol{Z}}(\boldsymbol{h}_l) = E\{[\boldsymbol{Z}(\boldsymbol{x}) - \boldsymbol{Z}(\boldsymbol{x}+\boldsymbol{h}_l)][\boldsymbol{Z}(\boldsymbol{x}) - \boldsymbol{Z}(\boldsymbol{x}+\boldsymbol{h}_l)]^T\} = \\ = \begin{bmatrix} \gamma_{11}^{\boldsymbol{Z}}(\boldsymbol{h}_l) & \cdots & \gamma_{1P}^{\boldsymbol{Z}}(\boldsymbol{h}_l) \\ \vdots & \ddots & \vdots \\ \gamma_{P1}^{\boldsymbol{Z}}(\boldsymbol{h}_l) & \cdots & \gamma_{PP}^{\boldsymbol{Z}}(\boldsymbol{h}_l) \end{bmatrix}, l = 1, \dots, L$$

where L is the number of lags. $E$ and superscript $T$ are the expectation and transposition, respectively, and $\gamma_{ij}^{Z}(\boldsymbol{h}_l)$is cross-variogram between $Z_i(\boldsymbol{x})$ and $Z_j(\boldsymbol{x})$ at lag distance $\boldsymbol{h}_l$.

Consider a $P \times P$ full rank matrix $\boldsymbol{W}$ that linearly transforms the random function $\boldsymbol{Z}(\boldsymbol{x})$ into factors $\mathrm{Y}(\boldsymbol{x}) = [Y_1(\boldsymbol{x}), Y_2(\boldsymbol{x}), \dots, Y_P(\boldsymbol{x})]$ with $\boldsymbol{Y}(\boldsymbol{x}) = \boldsymbol{Z}(\boldsymbol{x})\boldsymbol{W}$ such that $2\boldsymbol{\Gamma}_Y(\boldsymbol{h})$ is approximately diagonal for all distances $\boldsymbol{h}$. Then the problem is to find the transformation matrix $\boldsymbol{W}$ such that geostatistical simulation is performed independently on each of $Y_1(\boldsymbol{x}), \dots, Y_P(\boldsymbol{x})$ and the simulated factors $\boldsymbol{Y_S}(\boldsymbol{x})$ are back transformed into the original simulations by $\boldsymbol{Z_S}(\boldsymbol{x}) = \boldsymbol{Y_S}(\boldsymbol{x})\boldsymbol{W}^{-1}$. To guarantee the orthogonality of the transformation matrix, one can assume that the original data are whitened through principal component analysis before running the MSC method and the results are restricted to a unit circle [30]. In the rest of the paper, the white components will be denoted by $\boldsymbol{Z}(\boldsymbol{x})$ for simplicity.

### 2.2. Minimum Spatial Cross-correlation Method

Consider $\tau(\boldsymbol{h}) = \frac{\varphi(\boldsymbol{h})}{\xi(\boldsymbol{h})}$ , $|\boldsymbol{h}| > 0$

with $\varphi(h) = \sum_{i=1}^{p}\sum_{j\neq i}^{p}|\gamma_{ij}^{Y}(\boldsymbol{h})|$ and $\xi(\boldsymbol{h})$ =$\sum_{i=1}^{p}\gamma_{ii}^{Y}(\boldsymbol{h})$ as a measure of orthogonality. This measure is proposed by Tercan (1999) and is used by several researchers such as Mueller and Ferreira (2012) and Boluwade and Madramootoo (2015). This is also a measure considered in MSC method as the function to be minimized. $\tau(\boldsymbol{h})$ basically compares the sum of off-diagonal elements of factor variogram matrix to the sum of its diagonal elements at each lag distance. Efficient orthogonalization methods give factors with $\tau(\boldsymbol{h})$ values close to zero at all distances. Sohrabian and Tercan (2014a) prove that under a linear transformation of the variables with the same variance, $\xi(\boldsymbol{h})$ is constant at each lag distance. Then the problem of minimizing $\tau(\boldsymbol{h})$ is reduced to minimizing

$$\varphi = \sum_{l=1}^{L}\sum_{i=1}^{p-1}\sum_{i<j}^{p}|\gamma_{ij}^{Y}(\boldsymbol{h}_l)|, \qquad |\boldsymbol{h}| > 0 \tag{1}$$

Where $L$ is the number of lags considered in the minimization process. Cross variogram functions of factors lay between 1 and -1 due to whitening the input data and absolute values of these functions are not differentiable at some points in their domains so that $|\gamma_{ij}^{Y}(h_l)|$ can be replaced by $(\gamma_{ij}^{Y}(h_l))^2$ without changing in the directions. This translates Eq. 1 into the following one:

$$\varphi = \sum_{l=1}^{L}\sum_{i=1}^{p-1}\sum_{i<j}^{p}(\gamma_{ij}^{Y}(\boldsymbol{h}_l))^2, \qquad |\boldsymbol{h}| > 0 \tag{2}$$

Sohrabian and Tercan (2014a) show that such a complicated problem can be solved as a sequence of simplified 2-D problems with one parameter. For this purpose, we first minimize Eq. (2) in the plane, which consists of the first and second variables, and then proceeds in the other planes one by one. For illustration, the minimization problem is solved in 2-D space with one parameter $\theta_{12}$ for the following variogram matrix:

$$\boldsymbol{\Gamma_Z}(\boldsymbol{h}_l) = \begin{bmatrix} \gamma_{11}^{\boldsymbol{Z}}(\boldsymbol{h}_l) & \gamma_{12}^{\boldsymbol{Z}}(\boldsymbol{h}_l) \\ \gamma_{21}^{\boldsymbol{Z}}(\boldsymbol{h}_l) & \gamma_{22}^{\boldsymbol{Z}}(\boldsymbol{h}_l) \end{bmatrix} \tag{3}$$

The aim is to find a $2 \times 2$ transformation matrix $\boldsymbol{W}$

$$\boldsymbol{W} = \begin{bmatrix} cos\theta_{12} & -sin\theta_{12} \\ sin\theta_{12} & cos\theta_{12} \end{bmatrix} \tag{4}$$

to generate the factors using the following semi-variogram matrix:

$$\boldsymbol{\Gamma_Y}(\boldsymbol{h}_l) = \boldsymbol{W}(\theta_{12})^T\boldsymbol{\Gamma_Z}(\boldsymbol{h}_l)\boldsymbol{W}(\theta_{12}) = \begin{bmatrix} cos\theta_{12} & sin\theta_{12} \\ -sin\theta_{12} & cos\theta_{12} \end{bmatrix}\begin{bmatrix} \gamma_{11}^{\boldsymbol{Z}}(\boldsymbol{h}_l) & \gamma_{12}^{\boldsymbol{Z}}(\boldsymbol{h}_l) \\ \gamma_{21}^{\boldsymbol{Z}}(\boldsymbol{h}_l) & \gamma_{22}^{\boldsymbol{Z}}(\boldsymbol{h}_l) \end{bmatrix}\begin{bmatrix} cos\theta_{12} & -sin\theta_{12} \\ sin\theta_{12} & cos\theta_{12} \end{bmatrix} \\ = \begin{bmatrix} cos^2\theta_{12}\,\gamma_{11}^{\boldsymbol{Z}}(\boldsymbol{h}_l) + sin^2\theta_{12}\,\gamma_{22}^{\boldsymbol{Z}}(\boldsymbol{h}_l) + 2cos\theta_{12}sin\theta_{12}\,\gamma_{12}^{\boldsymbol{Z}}(\boldsymbol{h}_l) & cos\theta_{12}sin\theta_{12}(\gamma_{22}^{\boldsymbol{Z}}(\boldsymbol{h}_l) - \gamma_{11}^{\boldsymbol{Z}}(\boldsymbol{h}_l)) + (cos^2\theta_{12} - sin^2\theta_{12})\gamma_{12}^{\boldsymbol{Z}}(\boldsymbol{h}_l) \\ cos\theta_{12}sin\theta_{12}(\gamma_{22}^{\boldsymbol{Z}}(\boldsymbol{h}_l) - \gamma_{11}^{\boldsymbol{Z}}(\boldsymbol{h}_l)) + (cos^2\theta_{12} - sin^2\theta_{12})\gamma_{12}^{\boldsymbol{Z}}(\boldsymbol{h}_l) & cos^2\theta_{12}\,\gamma_{22}^{\boldsymbol{Z}}(\boldsymbol{h}_l) + sin^2\theta_{12}\,\gamma_{11}^{\boldsymbol{Z}}(\boldsymbol{h}_l) - 2cos\theta_{12}sin\theta_{12}\,\gamma_{12}^{\boldsymbol{Z}}(\boldsymbol{h}_l) \end{bmatrix} \tag{5}$$

Then the objective function to be minimized is:

$$\varphi(\theta_{12}) = \sum_{i=1}^{l}[\gamma_{12}^{Y}(\boldsymbol{h}_l)]^2 = \sum_{i=1}^{l}[cos\theta_{12}sin\theta_{12}(\gamma_{22}^{Z}(\boldsymbol{h}_l) - \gamma_{11}^{Z}(\boldsymbol{h}_l)) + (cos^2\theta_{12} - sin^2\theta_{12})\gamma_{12}^{Z}(\boldsymbol{h}_l)]^2 \tag{6}$$

Eq. (6) has only one parameter, $\theta_{12}$, which can be easily found by gradient descent algorithm that is based on iteration (7). The big disadvantage of gradient descent algorithm is the possibility of finding a local minimum rather than the global one. Sohrabian (2013) shows that $[\gamma_{12}^{Y}(\boldsymbol{h}_l)]^2$ has global minimum points repeated every 1.57 radians, removing the possibility that the function is trapped in a local optimum point.

Then consider the following iteration:

$$\theta_{12}^{t} = \theta_{12}^{t-1} - \zeta\left.\frac{\partial\varphi(\theta_{12})}{\partial\theta_{12}}\right|_{\theta_{12}=\theta_{12}^{t-1}} \tag{7}$$

Where $t$ is the currently calculated value of $\theta_{12}$, $t-1$ is the value of $\theta_{12}$ found at the previous step and $\zeta$ is the length of step in the negative gradient direction.

$$\frac{\partial\varphi(\theta_{12})}{\partial\theta_{12}} = \frac{\partial\sum_{l=1}^{L}(\gamma_{12}^{\boldsymbol{Y}}(\boldsymbol{h}_l))^2}{\partial\theta_{12}} = \\ = \sum_{l=1}^{L}[(cos^3\theta_{12}sin\theta_{12} - sin^3\theta_{12}cos\theta_{12})(2K_l^2 - 8(\gamma_{12}^{\boldsymbol{Z}}(\boldsymbol{h}_l))^2) \\ + 2K_l(cos^4\theta_{12} + sin^4\theta_{12} - 6 \\ \times cos^2\theta_{12}sin^2\theta_{12})\gamma_{12}^{\boldsymbol{Z}}(\boldsymbol{h}_l)] \quad (8)$$

Where $K_l = \gamma_{22}^{\boldsymbol{Z}}(\boldsymbol{h}_l) - \gamma_{11}^{\boldsymbol{Z}}(\boldsymbol{h}_l)$ (See [28] for the proof). Iteration (7) stops when $|\theta_{12}^{t} - \theta_{12}^{t-1}|$ falls below a tolerance level. After finding $\theta_{12}$, $\theta_{13}$, ..., $\theta_{1p}$, $\theta_{23}$, $\theta_{24}$, ..., $\theta_{2p}$, ... and $\theta_{pp}$, the final orthogonal transformation matrix that transforms $p$ stationary variables into the MSC factors is calculated as the multiplication of $p \times (p-1)/2$ distinct matrices $\boldsymbol{A}_{p\times p}(\theta_{ij}), i = 1, \dots, p-1$ and $j = i+1, \dots, p$ as shown in Eq. 9.

$$\boldsymbol{W}_{p\times p} = \prod_{i=1}^{p-1}\prod_{j=i+1}^{p}\boldsymbol{A}_{p\times p}(\theta_{ij}) \\ = \boldsymbol{A}_{p\times p}(\theta_{12}) \times \boldsymbol{A}_{p\times p}(\theta_{13}) \times \dots \times \boldsymbol{A}_{p\times p}(\theta_{(p-1)p}) \\ = \begin{bmatrix} cos\theta_{12} & -sin\theta_{12} & 0 & \cdots & 0 & 0 \\ sin\theta_{12} & cos\theta_{12} & 0 & \cdots & 0 & 0 \\ 0 & 0 & 1 & \cdots & 0 & 0 \\ \vdots & \vdots & \vdots & \ddots & \vdots & \vdots \\ 0 & 0 & 0 & \cdots & 1 & 0 \\ 0 & 0 & 0 & \cdots & 0 & 1 \end{bmatrix} \\ \times \begin{bmatrix} cos\theta_{13} & 0 & -sin\theta_{13} & 0 & \cdots & 0 \\ 0 & 1 & 0 & 0 & \cdots & 0 \\ sin\theta_{13} & 0 & cos\theta_{13} & 0 & \cdots & 0 \\ 0 & 0 & 0 & 1 & \cdots & 0 \\ \vdots & \vdots & \vdots & \vdots & \ddots & \vdots \\ 0 & 0 & 0 & 0 & \cdots & 1 \end{bmatrix} \times \cdots \\ \times \begin{bmatrix} 1 & 0 & \cdots & 0 & 0 & 0 \\ 0 & 1 & \cdots & 0 & 0 & 0 \\ \vdots & \vdots & \ddots & \vdots & \vdots & \vdots \\ 0 & 0 & \cdots & 1 & 0 & 0 \\ 0 & 0 & \cdots & 0 & cos\theta_{(p-1)p} & -sin\theta_{(p-1)p} \\ 0 & 0 & \cdots & 0 & sin\theta_{(p-1)p} & cos\theta_{(p-1)p} \end{bmatrix} \quad (9)$$

After producing the MSC factors in this way, their variograms are analyzed and the resulting variogram parameters are used to run the univariate geostatistical simulation method. Then the simulated factors are transformed back into the original data space. The main steps of the joint simulation of inter-correlated variables using the MSC factors are presented by the flowchart illustrated in Fig. 1.

## 3. Case Study

### *3.1. Field and geological setting description*

The data used in this study come from a part of the Ömerler sector of the Tunçbilek coalfield located in the western part of Turkey. Tunçbilek is a district of Tavşanlı–Kütahya and the Ömerler coal field is located in the northern part of Tunçbilek (Fig. 2). Tercan et al., (2013) carried out a complete seam modeling and resource estimation study in this field. Ertunç et al., (2013) estimated the coal quality means of the blocks by covariance matched constrained kriging and compared the results with the ordinary kriging estimates and geostatistical simulations.

Fig. 3 shows the generalized stratigraphic section of the coal basin. The following description of the Tunçbilek basin is largely based on Karayigit and Celik (2003). The Tunçbilek Neogene basin is situated between Tunçbilek and Domaniç (Kütahya) in the northeastern part of a horst–graben system in western Turkey. The metamorphic and ophiolitic rocks and granites of the Pre-Neogene age form the basement of the basin. The coal-bearing Tunçbilek Formation in the basin was conformably underlain by fluvial deposits of the Miocene Beke Formation and conformably overlain by sandstone–tuffite of the Miocene Besiktepe Formation and Pliocene volcanic rocks, fluvial–lacustrine deposits. The coal-bearing Tunçbilek Formation was developed in lacustrine facies (mudstone, claystone, coal, and marl), continental deltaic conglomerate–sandstone, continental fan deltaic conglomerate– sandstone–mudstone, and lacustrine limestone. The overall thickness of the Miocene–Pliocene formations in the basin is above 1 km.

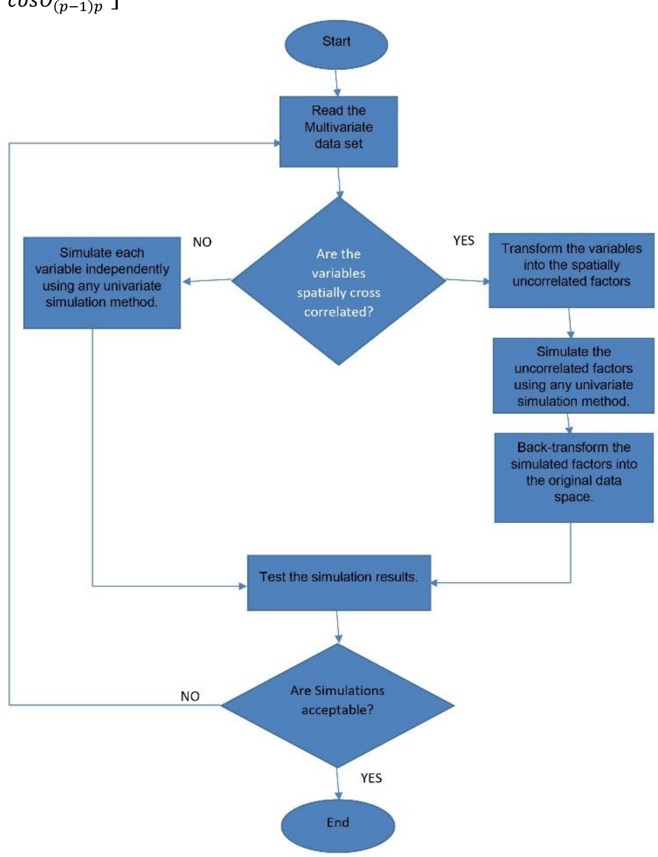


**Fig. 1.** Flowchart of the joint simulation using the MSC factors.

An average 7 m thick coal bed lies at the base of the Tuncbilek Formation. The coal bed lies between marl and conglomerate–sandstone units and includes dirt bands as claystone with coal traces, marl, and alternations of coal and claystone [34]. The coal seam dips with 7° in North-East direction.


Fig. 2. Location map of the Ömerler coal field. The mine site is shown by the yellow cross.

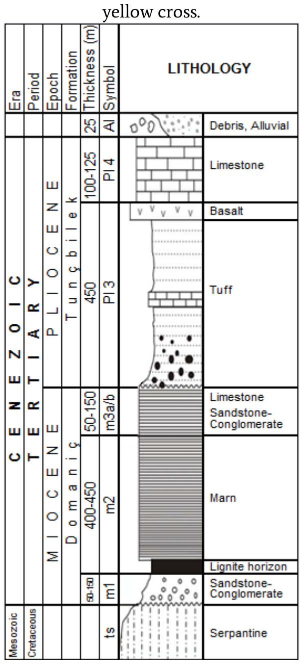


Fig. 3. Stratigraphic section of the basin.

### 3.2. Data, detrending and unfolding procedures

The study area contains 7 coal zones separated by NW-SE and N-S trending faults (Fig. 4). The data includes 115 bore-holes with samples analyzed for lower calorific value (LCV), ash content (AC) and moisture content (MC). The holes were drilled by the General Directorate of Turkish Coal Mining Administration (TKI) and the samples were collected from zones in which the drill-holes make intersect the coal bed and the coal samples were analyzed in the coal laboratory of Garp Lignite Operations (GLI). The laboratory uses ASTM D 5865-13 code (2016) for calorific value of coal and ASTM D 7582-15 code (2016) for proximate analysis. The drill-hole samples consist of only pure coal and do not include any parting so that the calorific value, ash content and moisture content of the partings are not known. In the Tunçbilek coal field LCV, AC and MC of the partings are assumed to be 1 kCal/kg, 75%, and 25% respectively as a standard application. We adopt this industry practice in our present study. These assumptions seem to be reasonable when we consider linear regression between the lower calorific value, and the ash content (not shown here) of all samples were analyzed if 1 kCal/kg is assumed as standard value for LCV of non-flammable substances.

The raw data are composed of 1 m intervals. While composting, the minimum rock parting is accepted to be 0.50 m and the previously assumed values of LCV, AC, and MC are used for the partings. Table 1 shows the summary statistics of the composites.

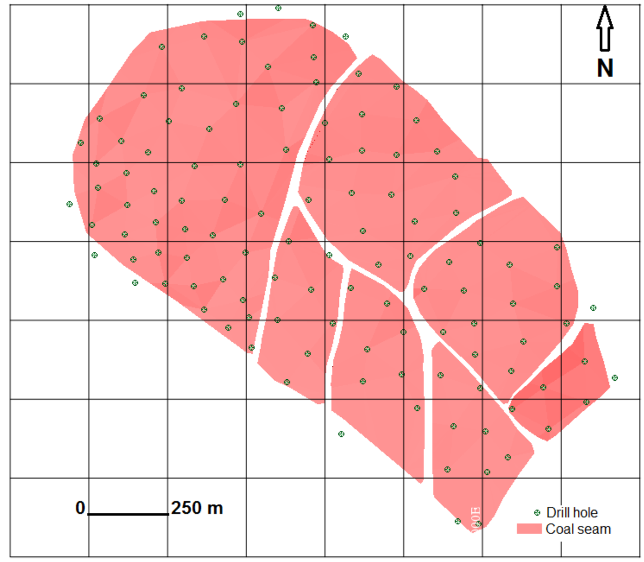


Fig. 4. Drill hole locations and the coal seam.

Table 1. The summary statistics of composite data.

| Variable | Number of composites | Min | Max | Mean | Variance |
|---|---|---|---|---|---|
| LCV(kCal/kg) | 620 | 925 | 5248 | 3239 | 1240183 |
| AC(%) | 620 | 9 | 64.52 | 35.95 | 187.88 |
| MC(%) | 620 | 11.50 | 25.11 | 18.46 | 8.30 |

The lignite seam of this study is faulted with throws of up to 20 m and strikes N50$^0$ W and dips 9$^0$ NE. Prior to the practical implementation of the MSC simulation, the seam and the composite data are unfolded to maintain the correct spatial relationships. For unfolding, the method suggested in Ertunç et al., (2013) is used. In addition, the lignite seam shows a vertical trend (Fig. 5) for coal quality variables due to decreasing the quality from the top of the seam to its bottom. To model the trend, the coal seam is divided into 2 m slices in the vertical direction and each slice is presented with a bar (Fig. 6). Then, the middle points of these bars are considered in the detrending process to obtain the second order stationary residuals to be used in generating the orthogonal factors through the MSC and the MAF approaches. The simulations are achieved in unfolded space using the detrending data. The simulations of the original data are obtained by adding the trend to the simulated residuals and transforming the unfolded coordinates into the original ones.

### 3.3. Joint simulation using the MSC factors and comparison to the MAF

After finding the residuals in the unfolded space, the principal component analysis and whitening process were implemented as pre-steps in generating the MSC factors. The maximum range of the cross-variograms (1000m) divided by the average distance of the adjacent drill holes (100m) was considered as the number of lags in the minimization process. The data-driven MAF method [14] was also implemented for comparison of the MSC-simulation to a more widely used technique. Two variogram matrices calculated at 200 m and 1000 m lag distances, which seem to be the ranges of the first and the second spatial structures were chosen for decorrelation. These matrices were checked to provide the requirements of the Cauchy–Schwarz inequality. After producing the factors using both methods, their orthogonality degree was tested regarding $\tau(h)$ measure [19].

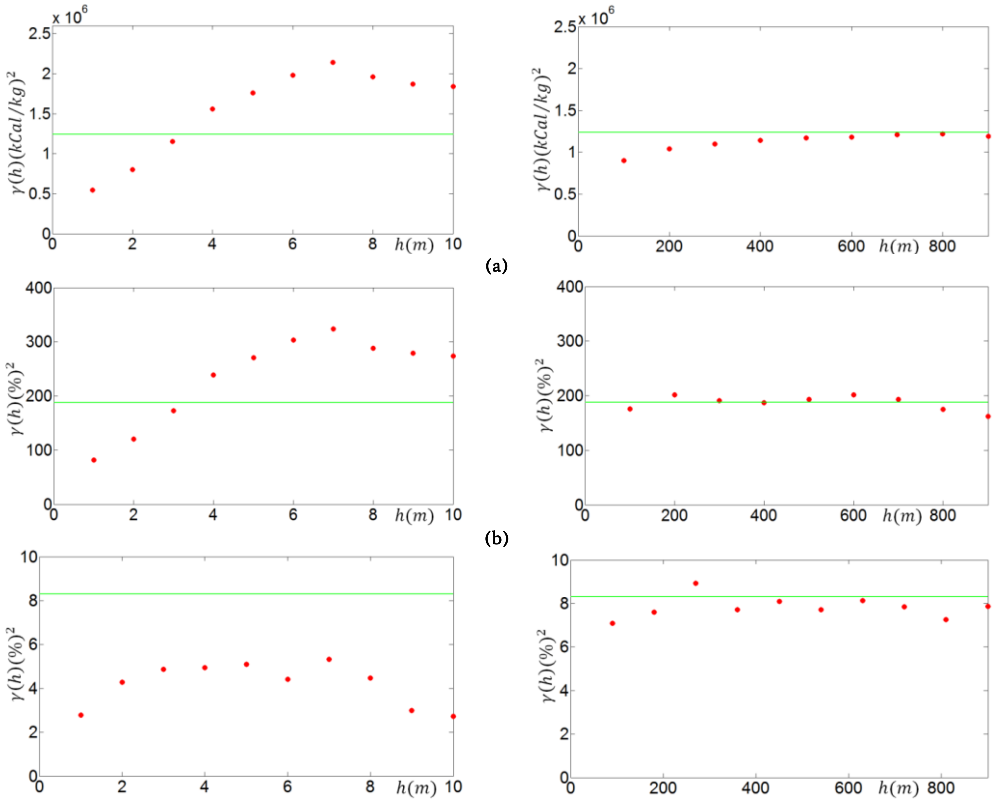

**Fig. 5.** Down-hole (left) and horizontal omnidirectional variograms (right) of; a) LCV, b) AC and c) MC.

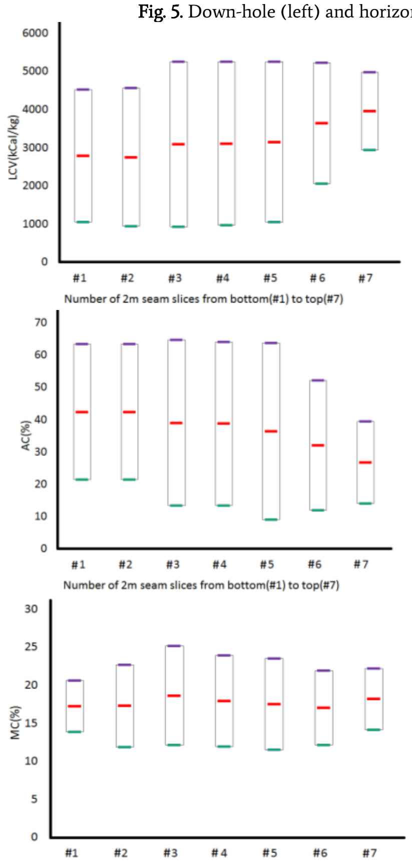

**Fig. 6.** Trend analysis of the coal attributes considering 2m seam slices from the bottom (#1) to the top (#7). Each slice is presented by a bar with the lowest and the highest values shown by green and purple lines. The middle points of the bars (Red line) are used in trend analysis.

Fig. 7 shows the cross-variograms and $\tau(h)$ values of the MSC and the MAF factors. Cross-variograms of the MAF factors are exactly equal to zero at decorrelation lag distances of 200m and 1000m and show a lower spatial correlation at short and long lags. But, for middle distances of 300m to 800m, where a large number of conditioning data is located, the MSC method demonstrates a better performance, which is confirmed by $\tau$ value. It can be said that all cross-variograms have negligible values such that the factors are practically orthogonal. This allows us to use any univariate geostatistical simulation method to generate the equiprobable realizations of the factors. Considering the histograms of the MSC and the MAF factors (Fig. 8) as well as running the Jarque–Bera test of normality at 5% significance level, it can be said that except for MSC1 and MAF3, the other factors possess non-Gaussian distributions. Then, Direct Sequential Simulation (DSS), through Soares approach [37], was implemented to generate 100 realizations for each factor on a grid of 120864 nodes within the boundaries of the coal seam.

The model variogram parameters fitted to the experimental variograms of factors (Fig. 9 and 10) are used in the simulations. Factors' vertical variogram ranges are less than their horizontal ranges, showing a geometrical anisotropy. Horizontal variograms of the MSC factors have sill values equal to their variances, but in down-hole direction, sill values of the variograms remain below the factor variances, indicating a zonal anisotropy. Therefore, they are fitted with nested models composed of a nugget effect and two spherical structures with very high ranges of the second structure (Table 2). Variograms of MAF1 and MAF3 are fitted with the same nested models, but using different ranges, nuggets, and contributions. Variograms of MAF2 are modeled with a nugget effect, and an exponential structure (Table 2). Simulations are carried out using 17 maximum conditioning data and applying search ellipsoids with axes 20% greater than the variogram ranges.

After simulating the MSC and MAF factors, the results are back-transformed into the original data space. Point support realizations are re-blocked to 3777 with block sizes of $50m \times 50m \times 1m$, and then, the MSC and the MAF-simulations are verified by comparing their cumulative density functions (cdf) (Fig. 11), correlation coefficients

(Fig.12), and auto/cross-variograms to those of the original data (Figs. 13 and 14). Fig. 11 shows that the MSC-simulations of variables could produce realizations with acceptable minimum and maximum values and reasonable cdf's. But, cdf reproduction of variables is poor for the MAF-simulations. Correlation coefficient reproduction of the MSC-simulations is better than the MAF-simulations and much closer to that of the data (Fig. 12). Figs. 13 and 14 show that the reproduction of variograms using the MAF-simulation is poor: auto-variograms of AC and LCV have respectively lower and higher nugget effects and sills. AC-MC and LCV-MC cross-variograms of MAF-simulations are consequently over and under those of the original data. On the other hand, the MSC-simulations show a good performance in variogram reproduction.

**Table 2.** Model variogram parameters of the MSC factors.

| Variable | MSC1 | MSC2 | MSC3 | MAF1 | MAF2 | MAF3 |
|---|---|---|---|---|---|---|
| Nugget | 0.45 | 0.15 | 0.22 | 0.2 | 0.1 | 0.4 |
| First structure | 0.35 | 0.25 | 0.38 | 0.5 | 0.9 | 0.35 |
| Second structure | 0.25 | 0.61 | 0.40 | 0.3 | - | 0.25 |
| Horizontal range 1 | 110 m | 200 m | 140 m | 130m | 230m | 100m |
| Horizontal range 2 | 400 m | 480 m | 300 m | 2500m | - | 400m |
| Vertical range 1 | 4.7 m | 6 m | 3.3 m | 12m | 13m | 4m |
| Vertical range 2 | 49 m | 200 m | 35 m | 500m | - | 150m |
| First structure's model | Sph | Sph | Sph | Sph | Exp | Sph |
| Second structure's model | Sph | Sph | Sph | Sph | - | Sph |

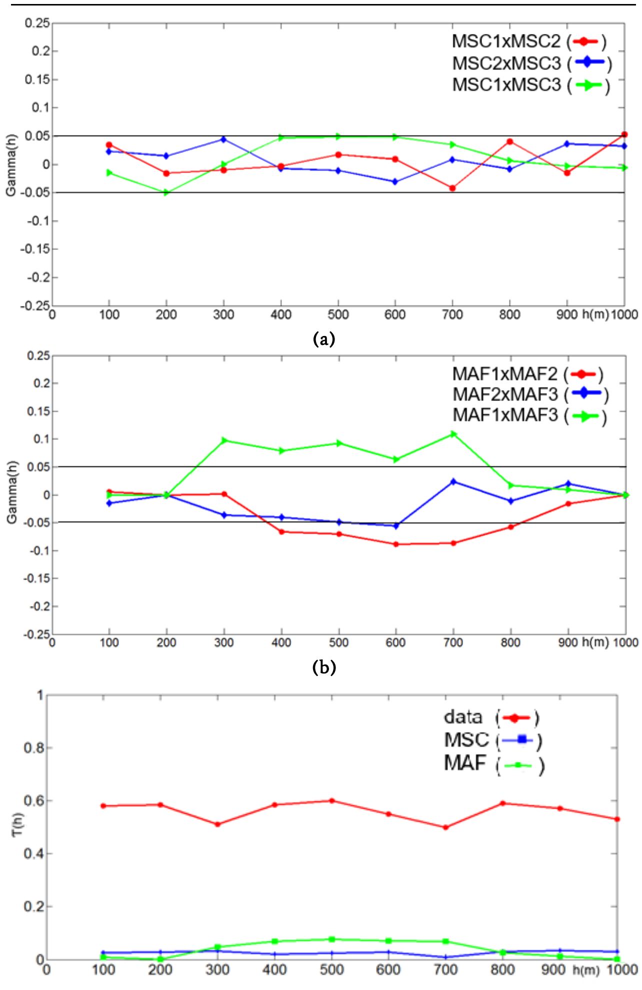


**Fig. 7.** Cross-variograms of; a) the MSC factors, b) the MAF factors, c) The measure of spatial orthogonality.

During this study, the MSC method was implemented by a MATLAB code written by the corresponding author, and the Stanford Geological Modeling Software (SGeMS) was used for variogram analysis and running the Direct Sequential Simulation.

### *3.4. Quality-tonnage curves and assessing uncertainty*

The Quality-tonnage curves were calculated using the MSC-simulations of variables and considering 9 different quantiles of the original data as the cutoff values (Fig. 15). Blocks with simulated values higher than each cutoff were considered in the tonnage and the average quality calculation. At each cutoff, the tonnages of 100 simulations were ranked from the smallest to largest values and the simulated tonnages falling at 95% symmetric confidence interval were used for the uncertainty quantification. In Fig. 14, the secondary axis shows the averages of the quality variables for blocks whose simulated values are considered above the cutoff. As the cutoff increases, the lignite tonnage decreases steadily. For example, a tonnage with LCV values equals to or above 2000 (kCal/kg) and 3000 (kCal/kg) lie in 10.5-12.1 and 7.7-9.8 million ton intervals respectively. There are similar relationships between the tonnage and cutoff values for AC and MC. For all variables, 95% confidence intervals are tighter for low and high cutoffs than the intermediate ones. LCV and AC have the lowest and the highest uncertainties in their quality- tonnage curves. This has important consequences in coal resource estimation, particularly in resource classification. By a simple change in the cut-off value, part of the resources might shift from one category to another. For example, the confidence in resource estimation at median cutoffs will be relatively low due to increasing the variability of simulated tonnages while it will be high at low and high cutoffs. This also affects mine planning, based on classified resources.

## 4. Conclusions

Uncertainty assessment for coal quality-tonnage curves is significant in all stages of a mining operation. For spatially inter-correlated variables, these curves can be calculated using the results of multivariate Geostatistical simulations. In this paper, an efficient joint simulation through the MSC factors was used to simulate the multivariate coal quality data of the Ömerler sector of the Tunçbilek coal field. This method shows several advantages over the joint simulation using the MAF factors and simplifies the multivariate simulation by producing spatially uncorrelated factors that are simulated independently.

As it was theoretically expected, the generated MSC factors are approximately orthogonal at all lag distances, so that the tedious procedure of cross-variograms modeling is removed. In comparison to the MAF factors, cross-variograms of the MSC factors lie in a tighter interval than those of MAFs. Moreover, as for the MAF approach, the MSC produces factors that are spatially autocorrelated and can be easily modeled. The generated factors are not necessarily normally distributed and their variograms show both geometrical and zonal anisotropies. The MSC-simulation method outperforms a joint simulation using the MAF factors by better reproduction of data's auto/cross-variograms, correlation coefficients and cumulative density functions so that their quality-tonnage curves are reliable. Due to lower variations in the generated realizations of LCV, LCV-tonnage curves show lower risk than AC-tonnage and MC-tonnage curves and fall in tighter intervals.

For being convenient, user-friendly as well as giving reliable results, we suggest implementing the joint simulation using the MSC factors regarding the following issue: this method is proposed for equally sampled data where variables are analyzed at all sample locations. For partial heteropy cases where multivariate data share some sample locations, it is necessary to either discard the incomplete samples or take advantages of imputation methods to obtain a complete isotopic data. Moreover, a vector of weights can be multiplied into the equations as some lags might have more importance to us because of some geological reasons or simply having more pair of points.

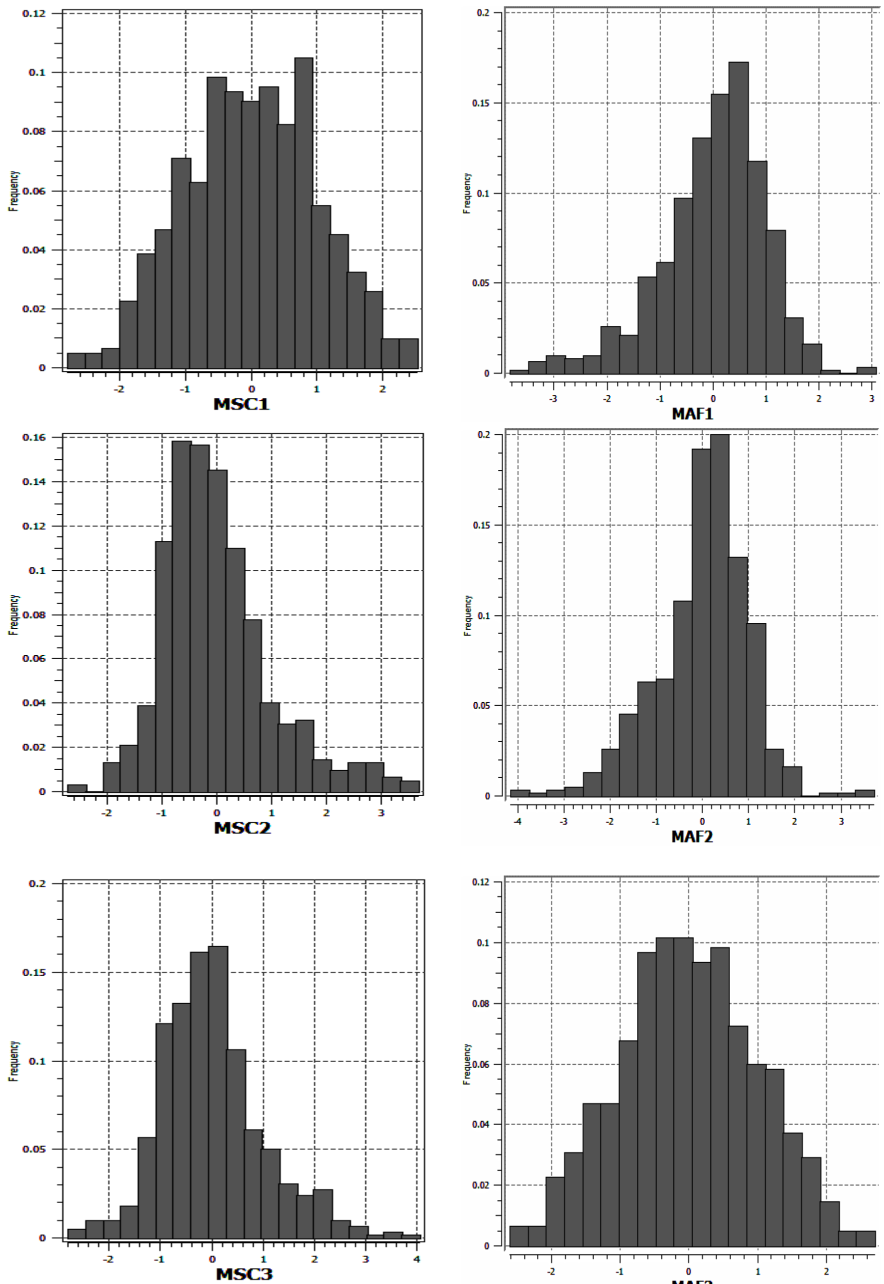


Fig. 8. Histograms of the MSC and the MAF factors.

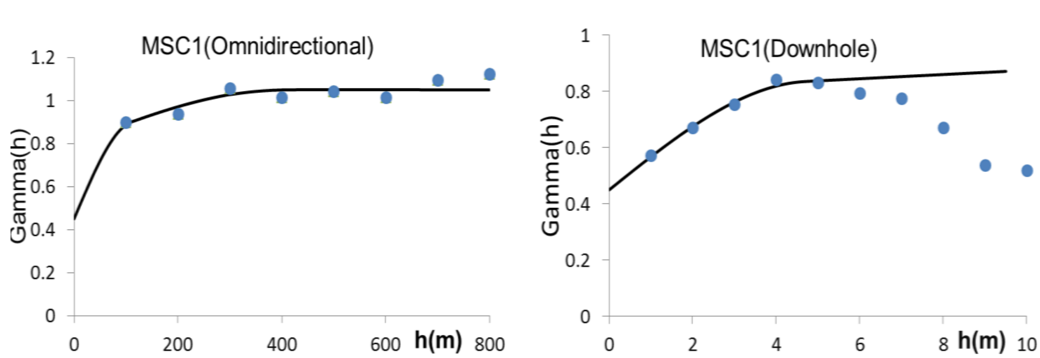

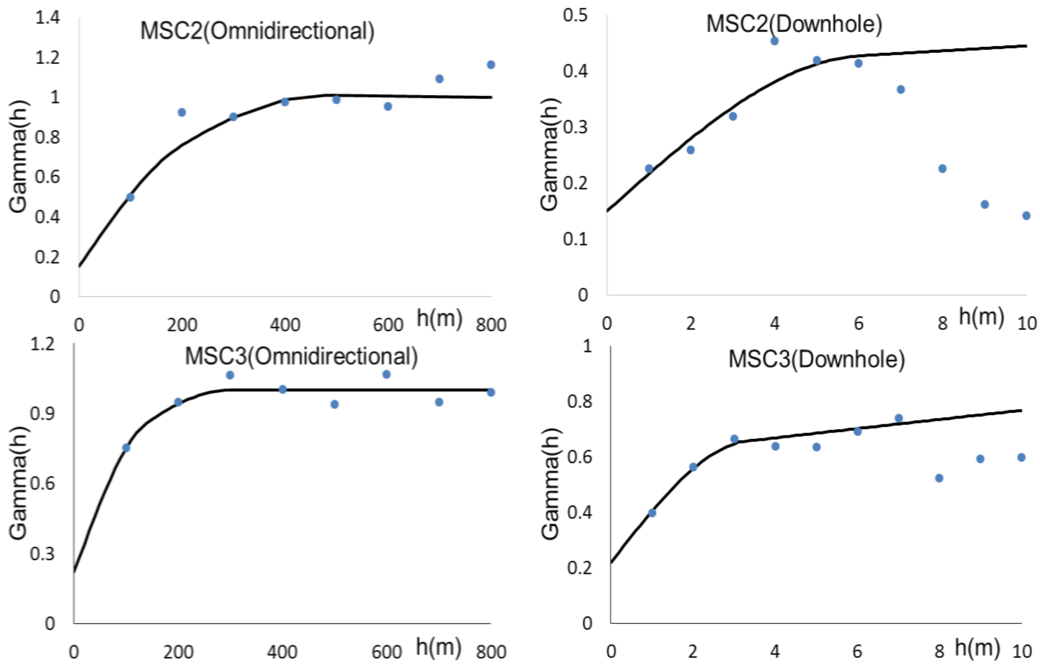


Fig. 9. Experimental variograms of the MSC factors (blue dots) together with the fitted models (black solid line).

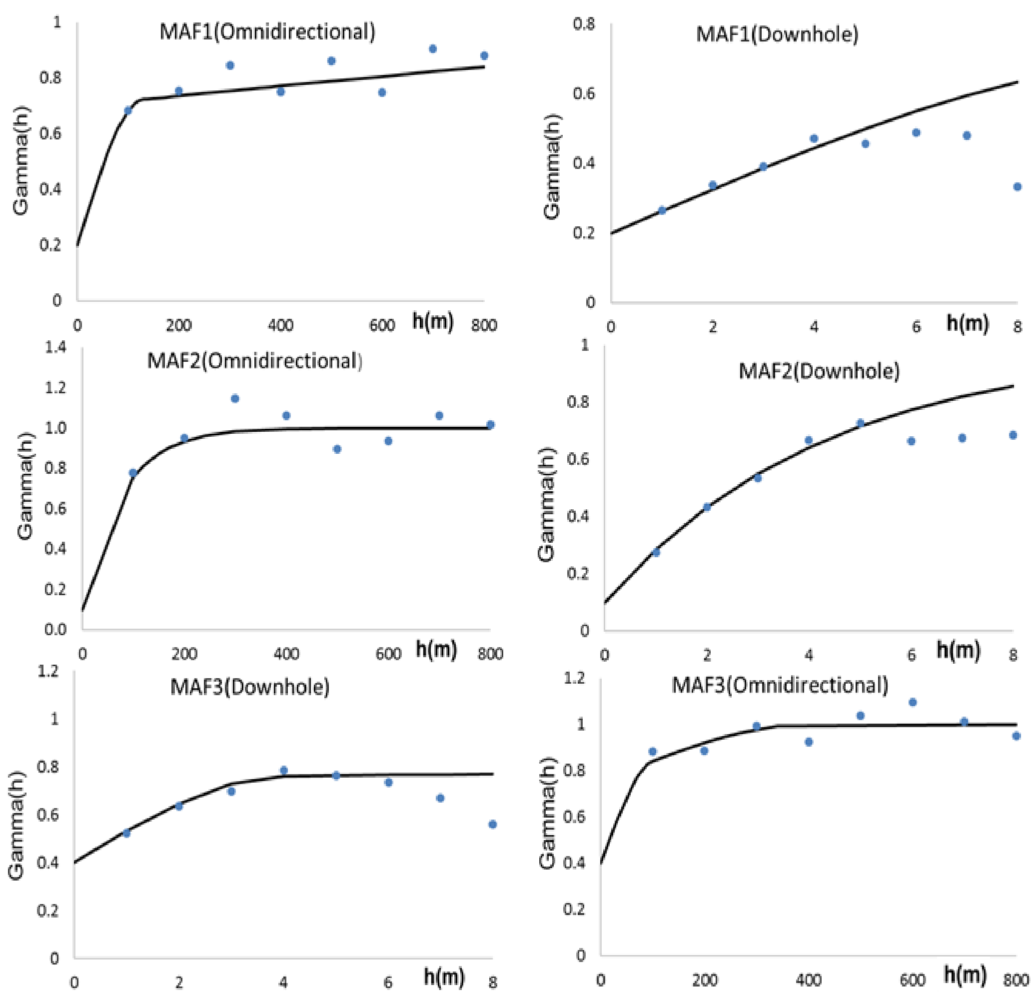


Fig. 10. Experimental variograms of the MAF factors (blue dots) together with the fitted models (black solid line).

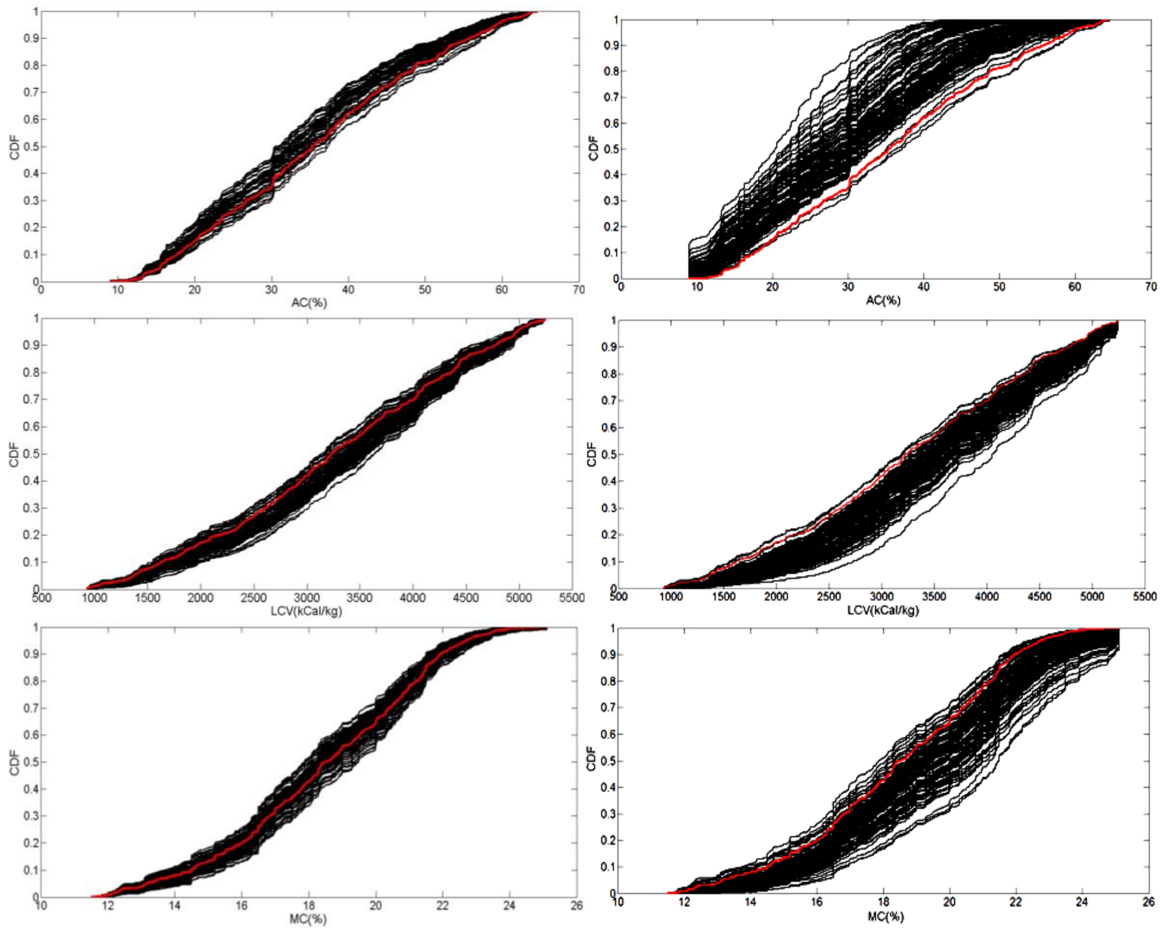


**Fig. 11.** Cumulative density functions of the MSC (left) and the MAF (right) simulations. The red and the black solid lines are consequently for the coal quality data and the simulations.

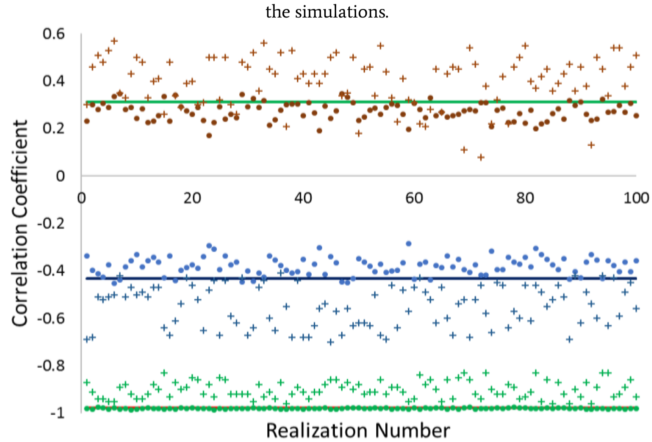


**Fig. 12.** Correlation coefficients of the simulations. Dot and Plus marks are for MSC-simulations and MAF-simulations respectively: LCV-AC (green), LCV-MC (blue) and AC-MC (brown). The targeted values are shown by solid lines.

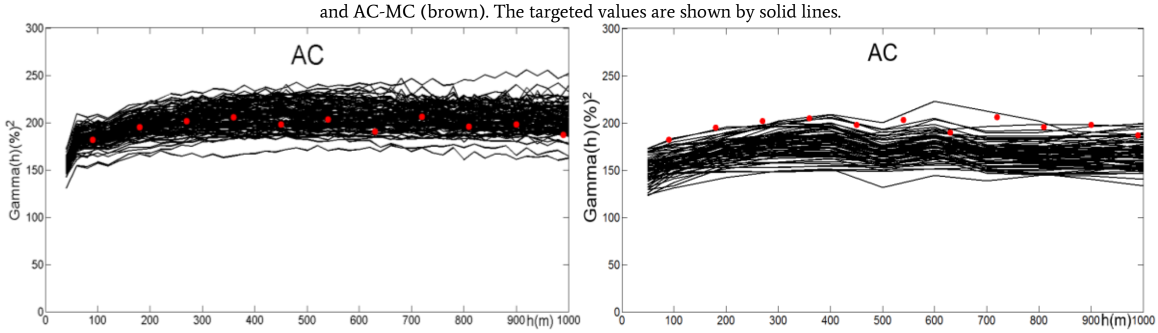

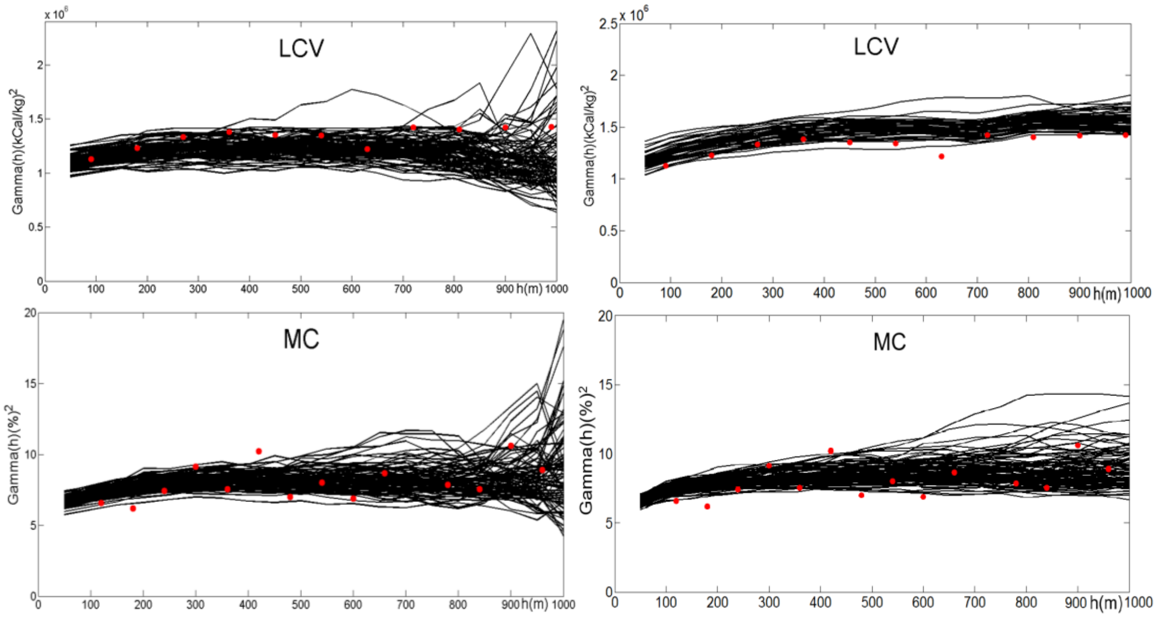


**Fig. 13.** Auto-variograms of the MSC (left) and MAF (right) simulations (Solid black lines) together with that of data (Red dots).

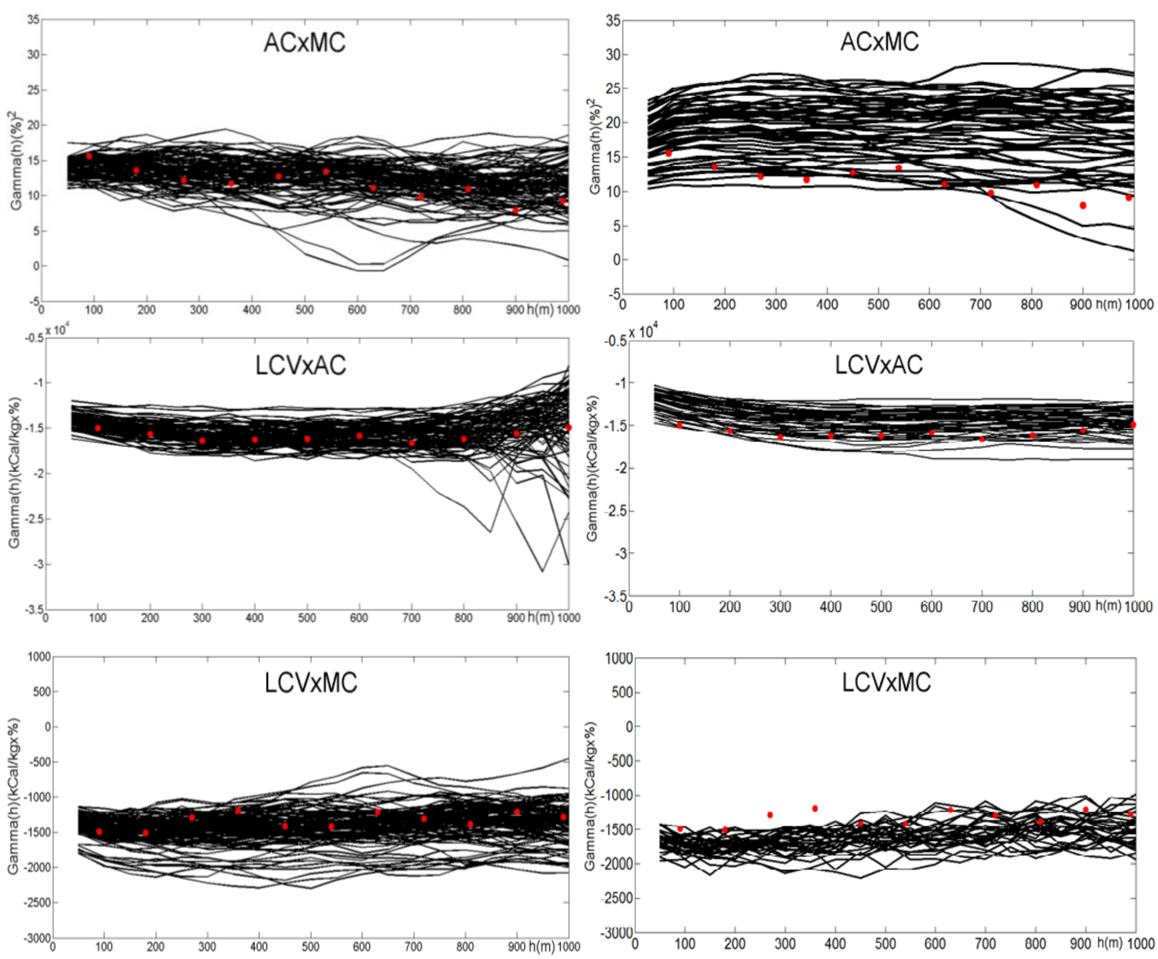


**Fig. 14.** Cross-variograms of the MSC (left) and the MAF (right) simulations (Solid black lines) together with that of data (Red dots).

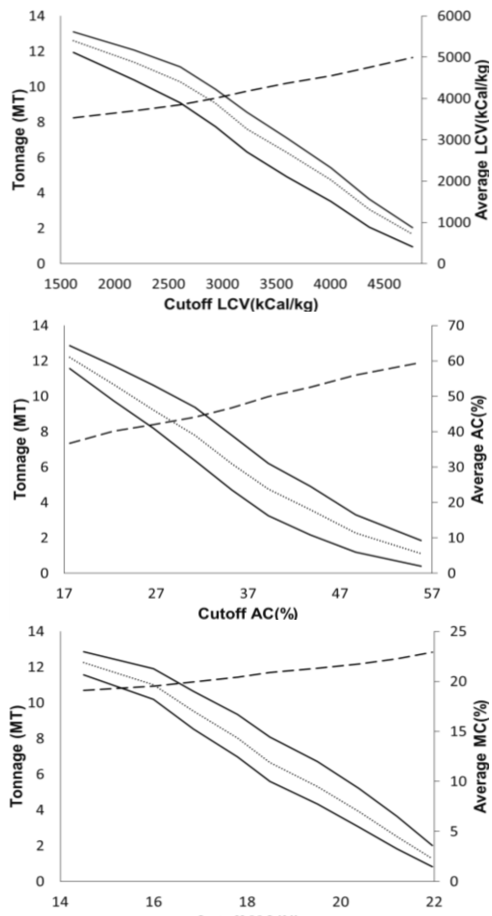


**Fig. 15.** Quality-tonnage curves of coal quality attributes. Symmetric 95% confidence interval (Solid Lines); median (dotted line); average quality (dashed line).

## REFRENCES


[1] Zawadzki, J., Fabijańczyk, P. & Badura, H., 2013. Estimation of methane content in coal mines using supplementary physical measurements and multivariable geostatistics. International Journal of Coal Geology, 118, pp.33–44. http://dx.doi.org/10.1016/j.coal.2013.08.005.

[2] Almeida, A.S. & Journel, A.G., 1994. Joint simulation of multiple variables with a Markov-type coregionalization model. Math Geol, 26(5), pp.565–588. Available at: http://dx.doi.org/10.1007/bf02089242.

[3] Emery, X., Silva, D. A., 2009. Conditional co-simulation of continuous and categorical variables for geostatistical applications. Computers & Geosciences, 35(6), 1234-1246.

[4] Yuan, C., Zhang, Z. & Liu, K., 2015. Assessment of the recovery and front contrast of CO2 EOR and sequestration in a new gas condensate reservoir by compositional simulation and seismic modeling. Fuel, 142, pp.81–86. Available at: http://dx.doi.org/10.1016/j.fuel.2014.10.045.

[5] De Almeida, J.A., 2010. Modelling of cement raw material compositional indices with direct sequential cosimulation. Engineering Geology, 114(1-2), pp.26–33. Available at: http://dx.doi.org/10.1016/j.enggeo.2010.03.007.

[6] Gloaguen, E., Marcotte, D., Chouteau, M., & Perroud, H., 2005. Borehole radar velocity inversion using cokriging and cosimulation. Journal of Applied Geophysics, 57(4), 242–259. http://dx.doi.org/10.1016/j.jappgeo.2005.01.001.

[7] Goovaerts, P., 1997. Geostatistics for natural resources evaluation. Applied Geostatistics Series, Oxford University Press

[8] Chilès, J. –P., & Delfiner, P., 2012. Geostatistics: Modeling Spatial Uncertainty, Second ed., Wiley Series in Probability and Statistics, John Wiley & Sons, Inc., Hoboken, New Jersey, 699pp. ISBN:978-0-470-18315-1

[9] Pan, G., Gaard, D., Moss, K., & Heiner, T. (1993). A comparison between cokriging and ordinary kriging: Case study with a polymetallic deposit. Mathematical Geology, 25(3), 377–398. doi:10.1007/bf00901424

[10] Davis, B.M. & Greenes, K.A., 1983. Estimation using spatially distributed multivariate data: An example with coal quality. Mathematical Geology, 15(2), pp.287–300. Available at: http://dx.doi.org/10.1007/bf01036071.

[11] Desbarats, A.J., Dimitrakopoulos, R., 2000. Geostatistical simulation of regionalized pore-size distributions usingmin/max autocorrelation factors.Mathematical Geology 32 (8), 919–941.

[12] Rondon, O., 2011. Teaching Aid: Minimum/Maximum Autocorrelation Factors for Joint Simulation of Attributes. Math Geosci, 44(4), pp.469–504. Available at: http://dx.doi.org/10.1007/s11004-011-9329-6.

[13] Lopes, J.A., Rosas, C.F., Fernandes, J.B., Vanzela, G.A., 2011. Risk quantification in grade–tonnage curves and resource categorization in a lateritic nickel deposit using geologically constrained joint conditional simulation. Journal of Mining Science 47 (2), 166–176. doi:10.1134/S1062739147020043.

[14] Sohrabian, B. & Ozcelik, Y., 2012a. Joint simulation of a building stone deposit using minimum/maximum autocorrelation factors. Construction and Building Materials, 37, pp.257–268. Available at: http://dx.doi.org/10.1016/j.conbuildmat.2012.07.033.

[15] Tajvidi, E. et al., 2013. Application of joint conditional simulation to uncertainty quantification and resource classification. Arab J Geosci, 8(1), pp.455–463. Available at: http://dx.doi.org/10.1007/s12517-013-1133-9.

[16] Leuangthong, O., Deutsch, C.V., 2003. Stepwise Conditional Transformation for Simulation of Multiple Variables, Mathematical Geology, Volume 35, Issue 2, pp 155-173.

[17] Hosseini, S.A., Asghari, O., 2015. Simulation of geometallurgical variables through stepwise conditional transformation in Sungun copper deposit, Iran. Arabian Journal of Geosciences, 8(6), 3821-3831.

[18] Mueller, U.A. & Ferreira, J., 2012. The U-WEDGE Transformation Method for Multivariate Geostatistical Simulation. Math Geosci, 44(4), pp.427–448. Available at: http://dx.doi.org/10.1007/s11004-012-9384-7.

[19] Tercan, A.E., 1999. Importance of orthogonalization algorithm in modeling conditional distributions by orthogonal transformed indicator methods. Math. Geol. 31 (2), 155–173.

[20] Xie, T., Myers, D.E. & Long, A.E., 1995. Fitting matrix-valued variogram models by simultaneous diagonalization (Part II: Application). Math Geol, 27(7), pp.877–888. Available at: http://dx.doi.org/10.1007/bf02087101.

[21] Sohrabian, B., Ozcelik, Y., 2012b. Determination of exploitable blocks in an andesite quarry using independent component kriging. Int. J. Rock Mech. Min. Sci. 55, 71-79.

[22] Tercan, A.E., Sohrabian, B., 2013. Multivariate geostatistical simulation of coal quality data by independent components. Int. J. Coal Geol. 112, 53–66.

[23] Boluwade, A., Madramootoo, C.A., 2015. Geostatistical independent simulation of spatially correlated soil variables. Computers & Geosciences, 85, 3-15.

[24] Ruessink, B.G ., van Enckevort, I. M.J ., & Kuriyama, Y. (2004). Non-linear principal component analysis of nearshore bathymetry. Marine Geology, 203(1-2), 185–197. doi:10.1016/s0025-3227(03)00334-7

[25] Nielsen, A. A. (2011). Kernel Maximum Autocorrelation Factor and Minimum Noise Fraction Transformations. IEEE Transactions on Image Processing, 20(3), 612–624. doi:10.1109/tip.2010.2076296

[26] Lio, S., Luo, M., Zhang, G. (2013). Face recognition based on symmetrical kernel principal component analysis. Journal of Computer Applications, 32(5), 1404–1406. doi:10.3724/sp.j.1087.2012.01404

[27] Musafer, G. N., & Thompson, M. H. (2016). Non-linear optimal multivariate spatial design using spatial vine copulas. Stochastic Environmental Research and Risk Assessment. doi:10.1007/s00477-016-1307-6

[28] Sohrabian, B., Tercan, A.E., 2014a. Introducing minimum spatial cross-correlation kriging as a new estimation method of heavy metal contents in soils, Geoderma, 226-227, 317-331. http://dx.doi.org/10.1016/j.geoderma.2014.02.014

[29] Sohrabian, B. & Tercan, A.E., 2014b. Multivariate geostatistical simulation by minimising spatial cross-correlation. Comptes Rendus Geoscience, 346(3-4), pp.64–74. http://dx.doi.org/10.1016/j.crte.2014.01.002.

[30] Hyvarinen, A., Karhunen, J., Oja, E., 2001. Independent Component Analysis. JohnWiley & Sons (481 pp.).

[31] Sohrabian, B., 2013. Bağımsız Bileşenler Analizi ile Çok Değişkenli Jeoistatistiksel Kestirim (in Turkish). PhD thesis. Hacettepe University, Ankara, Turkey. http://hdl.handle.net/11655/2842

[32] Tercan, A.E., Űnver, B., Hindistan, M.A., Ertunç, G., Atalay, F., Űnal, S., Kıllıoğlu, Y., 2013. Seam modelling and resource estimation in the coalfields of western Anatolia. International Journal of Coal Geology. Int. J. Coal Geol. 112, 94-106. http://dx.doi.org/10.1016/j.coal.2012.10.006.

[33] Ertunç, G., Tercan, A.E., Hindistan, M.A., Űnver, B., Űnal, S., Atalay, F., Kıllıoğlu, S.Y., 2013. Geostatistical estimation of coal quality variables by using covariance matching constrained kriging. International Journal of Coal Geology. Int. J. Coal Geol. 112, 14-25.

[34] Karayigit, A.I. & Celik, Y., 2003. Mineral Matter and Trace Elements in Miocene Coals of the Tuncbilek-Domanic Basin, Kutahya, Turkey. Energy Sources, 25(4), pp.339–355. Available at: http://dx.doi.org/10.1080/00908310390142370.

[35] ASTM D5865-13, 2016. Standard Test Method for Gross Calorific Value of Coal and Coke, ASTM International, West Conshohocken, PA, 2013, http://dx.doi.org/10.1520/D5865

[36] ASTM D7582-15, 2016. Standard Test Methods for Proximate Analysis of Coal and Coke by Macro Thermogravimetric Analysis, ASTM International, West Conshohocken, PA, 2015, http://dx.doi.org/10.1520/D7582-15

[37] Soares, A., 2001. Direct Sequential Simulation and Cosimulation Mathematical Geology, 33(8), pp.911–926. http://dx.doi.org/10.1023/a:1012246006212.